THE ASTROPHYSICAL JOURNAL, 545:874–884, 2000 December 20

CO OBSERVATIONS TOWARD SUPERNOVA REMNANTS WITH ASSOCIATED OH 1720 MHz MASERS

ESTELA M. REYNOSO[1]
Instituto de Astronomía y Física del Espacio, CC 67 Suc 28, (1428) Buenos Aires, Argentina
AND
JEFFREY G. MANGUM
National Radio Astronomy Observatory, 949 North Cherry Avenue, Tucson, AZ 85721-0655
Received 2000 May 11; accepted 2000 August 14

ABSTRACT

The environs of three supernova remnants (SNRs) with associated OH 1720 MHz masers, G349.7+0.2, CTB 37A, and G16.7+0.1, have been surveyed in the CO $J = 1$–0 transition with the 12 Meter Telescope of the NRAO, using the on-the-fly technique. These observations have revealed a number of molecular clouds interacting with the SNR shock fronts. Most of the OH 1720 MHz masers have been found to lie over CO concentrations, and the maser velocities are coincident with the CO peak velocities to an accuracy better than 2 km s^{-1}. The present data trace the interstellar medium (ISM) structures interacting with the SNRs; however, to probe the shocked molecular gas in which the OH 1720 MHz emission originates, higher excitation transitions and more complex species should be observed. In CTB 37A, where the shock velocity into the molecular cloud could be determined, it has been found to be of C-type, in agreement with theoretical predictions. Part of the rim of G16.7+0.1 appears to be flattened by a dense external cloud, yet the only associated OH 1720 MHz maser lies near the opposite region of the remnant. This behavior, also observed in IC 443 and 3C 391, seems to contradict the suggestion that OH 1720 MHz maser emission occurs mainly for transverse shocks.

Subject headings: ISM: clouds — ISM: individual (G349.7+0.2, CTB 37A, G16.7+0.1) — ISM: molecules — masers — supernova remnants

1. INTRODUCTION

When a supernova remnant (SNR) expands near or inside a molecular cloud, the shock driven into the cloud can accelerate relativistic particles, heat and compress the molecular gas, and change its chemistry, in addition to being an important source of turbulent mixing. If the turbulence is not strong enough to disrupt the cloud, condensed clumps may be created, which eventually may become new stars. Therefore, the interaction of SNRs with molecular clouds joins the two endpoints of the life cycle of stars and gas in our Galaxy (Frail, Goss, & Slysh 1994). The study of such interactions sheds light on several different fields in astrophysics.

Unfortunately, confusion introduced by unrelated gas along the line of sight makes it not trivial to establish unambiguously whether an SNR is physically associated with a molecular cloud or whether their distances differ and they appear as positionally coincident just because of a projection effect. Morphological signatures, such as arcs of gas outlining an SNR or indentations in SNR edges surrounding gas concentrations, are often used (Landecker et al. 1989; Reynoso et al. 1995; Dubner et al. 1999). More convincing, but also more rare, are line broadenings (e.g., Frail & Mitchell 1998; Reach & Rho 1999) or wings (Seta et al. 1998) indicative of shocked gas.

Almost three decades ago, Goss (1968) discovered for the first time OH emission in the satellite line at 1720 MHz associated with two SNRs: W28 and W44 (see also Goss & Robinson 1968). Hardebeck (1971) found that this emission comes from several compact regions with strong inversion of the OH levels. Later, another OH 1720 MHz emission feature was found towards IC 443 (DeNoyer 1979a). Turner (1969) suggested that the inversion of the 1720 MHz line is produced by infrared pumping. Since then, however, Galactic OH maser emission at 1720 MHz near SNRs has been largely forgotten. In the following years, the evidence that the three SNRs above are interacting with nearby clouds has grown as to make them three of the best-known and most-studied cases of SNR–molecular cloud interactions (e.g., Wootten 1977, 1981; DeNoyer 1979b, 1983; White et al. 1987; Burton et al. 1988). It is natural then to suggest that this interaction plays a key role in the production of maser emission at 1720 MHz (Frail et al. 1996). Several OH 1720 MHz surveys have been carried out recently (Frail et al. 1996; Green et al. 1997; Koralesky et al. 1998) in order to find new cases of SNR–OH 1720 MHz maser associations. At present, among 150 surveyed Galactic SNRs, positive results have been obtained for around 20 of them.

The origin of this maser emission can be easily explained through collisional excitation by the passage of a shock front (Frail et al. 1996). Therefore, the presence of OH 1720 MHz masers is proposed as a powerful tool to diagnose SNR–molecular cloud interactions. Elitzur (1976) showed that the pumping is more efficient if the kinetic temperature is in the range 25–200 K, and the H_2 density is in the range 10^3–10^5 cm^{-3}. Lockett, Gauthier, & Elitzur (1999) found tighter constrains on the physical conditions needed to produce OH 1720 MHz maser emission: the presence of masers imply moderate temperatures (50–125 K) and densities of the order of 10^5 cm^{-3}, which can exist only if the shocks are of C-type. Thus, the absence of OH 1720 MHz masers in itself is not enough to rule out an interaction. Since the maximum amplification occurs along the edge of an SNR, where the least velocity dispersion and hence the

[1] Member of the Carrera del Investigador Científico, CONICET, Argentina; ereynoso@iafe.uba.ar.

largest coherence is maintained, the velocity of an OH 1720 MHz maser associated to an SNR can be identified with the systemic velocity of the remnant, making it possible to constrain its distance. This property is also suggested by Claussen et al. (1997), who point out that the only OH 1720 MHz maser emission observed toward IC 443 appears at the site where clear evidence for the existence of a transverse shock is found.

In a recent paper, Frail & Mitchell (1998) surveyed the regions of the masers associated with the well-studied SNRs W28, W44, and 3C 391, in high-excitation CO and H_2CO transitions. The latter SNR is also known to be interacting with molecular gas (Wilner, Reynolds, & Moffett 1998; Reach & Rho 1998, 1999). The authors succeeded in finding the molecular shocks in all three of them, supporting the idea that the masers originate in postshock gas. They found that the masers are distributed near, but not coincident with, peaks of CO $J = 3$–2 emission.

Motivated by the proposed interaction between SNRs and molecular clouds that OH 1720 MHz masers may reveal, we have selected three SNRs: G349.7+0.2, G16.7+0.1, and CTB 37A, and surveyed the molecular gas around them in search for the clouds hypothetically interacting with the shock fronts. We used the lowest energy transition of the CO molecule as a probe, which is ubiquitous and easy to detect, as a first approach to the structure of the ISM around these remnants. The present observations allowed us to detect several sites of possible interaction between these SNRs and the surrounding molecular gas, even at locations where no OH 1720 MHz masers are present (e.g., G16.7+0.1). These observations provide the basis for future work analyzing molecular shocks through higher transitions, and for comparing the physics of shocked and unshocked gas.

2. OBSERVATIONS AND DATA REDUCTION

Observations of the CO $J = 1$–0 line (115.271204 GHz) were performed with the NRAO[2] 12 Meter Telescope located on Kitt Peak, Arizona, on 1998 June 12–18 and 27–30. The beam size at this frequency is 54″. A square field of $\sim 38' \times 38'$ was covered toward each of the remnants. Observations were made using the on-the-fly (OTF) technique, allowing efficient imaging of extended regions. Three different spectrometers were employed: two of them with 128 channels and resolutions of 1 MHz and 500 kHz, respectively, and a 768-channel correlator with a resolution of 98 kHz. An absolute position-switching mode was used, with reference positions given in Table 1. These reference positions were measured to be free of CO emission down to levels of less than about 0.5 K. Four images were obtained for G349.7+0.2, five for G16.7+0.1 and two for CTB 37A. Since data at the 12 Meter Telescope are calibrated by default to the T_R^* scale, which is equivalent to the radiation temperature T_R for a source much larger than the main diffraction beam of the telescope, it is often necessary to apply corrections that refer to sources of different sizes. For sources with sizes in the range 20″–40″, the efficiency factor which converts T_R^* to T_R is 0.85 based on historic measurements of the planets Jupiter and Saturn.

The AIPS package was employed for data processing. Baselines were subtracted in the raw data directly with the task SDLSF, which uses a unique range of line-free channels in the whole area. Because of the proximity of all three sources to the Galactic plane, the intensity distribution

[2] The National Radio Astronomy Observatory is a facility of the National Science Foundation operated under cooperative agreement by Associated Universities, Inc.

TABLE 1

OBSERVATIONAL PARAMETERS

A

Parameter	G349.7+0.2	CTB37A	G16.7+0.1
Central position			
R.A. (1950)	17 14 36.0	17 11 00.0	18 18 07.4
Decl. (1950)	−37 22 59	−38 30 00	−14 23 18
Reference position			
R.A. (1950)	17 00 36.0	16 35 00.0	18 35 07.4
Decl. (1950)	−37 22 59	−38 00 00	−14 23 18
Number of images	3	2	5
Observing time (hr)	4.1	3.6	8.3
Central velocity (LSR) (km s^{-1})	−40	−65	+50
rms (K)	0.6	0.8	0.3

B

Parameter	Value
Frequency (GHz)	115.27 (2.6 mm)
Spectral resolution (kHz, km s^{-1})	
autocorrelator	98, 0.25 (768)
spectrometer 1	500, 2.6 (128)
spectrometer 2	1000, 1.3 (128)
Angular resolution (arcsec)	53.6 × 53.6
Surveyed area (arcmin)	∼38 × 38
Observing mode	absolute position switching

NOTE.—In the "spectral resolution" line, the numbers in parentheses give the number of channels. Units of right ascension are hours, minutes, and seconds, and units of declination are degrees, arcminutes, and arcseconds.

along the observed images made it extremely difficult to find a suitable range of line-free channels. We thus decided to give priority to the baseline removal in the regions closest to the remnants and OH 1720 MHz masers, with possible detriment to the rest. Images were averaged for each source using the task WTSUM, with $1/\sigma^2$ as weight, where σ is the noise image corresponding to each image. Because of the very high noise of one of the original images of G349.7+0.2, only three of them were kept in the average for this source.

In Table 1, we summarize the observational parameters, including the noise of the final images for each SNR.

3. RESULTS

In what follows, we will devote a subsection to each SNR, including a brief introduction to the remnant, a description of our CO results and an estimation of physical parameters for the structures most probably related to the remnant. Distances shall be derived from the Galactic rotation model by Fich, Blitz, & Stark (1989). To calculate the H_2 column density, the relationship $X = N(H_2)/W_{CO}$ will be used, where W_{CO} is the integrated CO line intensity, $W_{CO} = \int T_R(CO)\,dv$, in K km s^{-1}, and where we have divided our antenna-based T_R^* temperatures by the efficiency factor of 0.85 to place them on the T_R scale appropriate for sources with sizes in the range 20″–40″. Several studies suggest a trend of increasing X with Galactocentric distance (Digel et al. 1997), thus the value of X may vary from one remnant to another.

Masses will be estimated by integrating N_{H_2} over the solid angle subtended by the CO emission feature. Assuming spherical volumes and using a mean molecular weight per H_2 molecule of 2.72 m_H (Allen 1973), the mass and density of a cloud can be expressed as

$$M = 5.65 \times 10^{-21}\, X W_{CO}\, \theta^2 D^2\, M_\odot \qquad (1)$$

and

$$n_{H_2} = \frac{4.1 \times 10^{-19}\, X W_{CO} \sqrt{f}}{D\theta}\ \mathrm{cm}^{-3}, \qquad (2)$$

where D is the distance in kpc, θ is the angular radius in arcminutes of the cloud assumed (spherical), computed as half the measured diameter deconvolved by the beam size, and f is a correction factor allowing for elongated shapes, and is given by the ratio $\theta_{maj}/\theta_{min}$.

3.1. *G349.7+0.2*

This remnant consists of an incomplete clumpy shell, 2′ in diameter, with enhancement to the south (Fig. 1). H I observations (Caswell et al. 1975) suggest that G349.7+0.2 is located beyond the tangent point, since absorption features are detected even at positive velocities, up to about +6 km s^{-1}. Clark & Caswell (1976) notice that the strong north-south emission ridge, somewhat east of the center, probably represents a nonuniform distribution of emission in a shell rather than a filled center, and would be evidence for a strong interaction with the ISM at an early stage in the life of this SNR. Frail et al. (1996) detected five OH 1720 MHz masers, with the brightest of them aligned along the emission ridge, and a few weak ones at the southern continuum knot.

Our CO observations clearly reveal a concentration inside the remnant, at R.A. = 17^{h}18^{m}0^s.0, decl. = −37°26′36″ (J2000). This concentration appears just above the southern knot, coincident with the emission ridge. A Gaussian fit to the spectrum of this cloud yields a central velocity of +16.5 km s^{-1} and a FWHM velocity of $\Delta v = 4$ km s^{-1}. Figure 2 shows the cloud integrated over this Δv. There is a striking coincidence among the CO cloud and the OH 1720 MHz masers, which appear encircling the former. From Table 2 in Frail et al. (1996), the velocities of the OH 1720 MHz masers vary from +14.3 to +16.9 km s^{-1}, in excellent agreement with the velocity of the CO cloud.

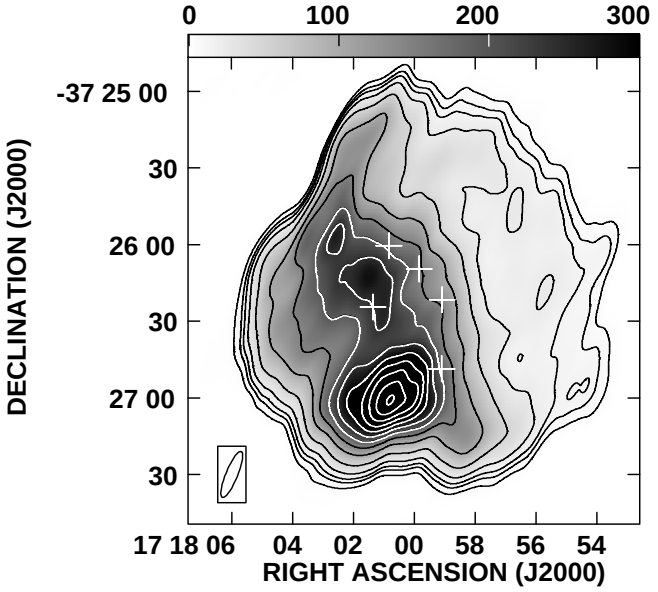

FIG. 1.—Radio continuum image of G349.7+0.2 at 1.4 GHz obtained with the VLA, kindly provided by C. Salter. The gray scale is indicated in mJy beam^{-1} on top of the image, while the contours are expressed as a percentage of the peak flux density (0.48 Jy beam^{-1}) at 1, 2, 3, 5, 10, 20, 30, 40, 50, 60, 70, 80, 90, and 99%. For better contrast, white contours are used over dark shadows. The white crosses show the positions of the OH 1720 MHz masers detected by Frail et al. (1996). The beam, indicated in the bottom left corner, is 19.″4 × 4.″5, P.A. = −22.°2.

If we adopt the systemic velocity of the cloud to be +16.5 km s^{-1}, the distance turns out to be ∼23 kpc, in close agreement with previous results (Frail et al. 1996). The diameter of the cloud is estimated to be ∼50″, which corresponds to 5 pc. This CO cloud is placed at a Galactocentric distance of $R = 14$ kpc. For $R = 12$–13 kpc, Digel, Bally, & Thaddeus (1990) estimate that $X = (8 \pm 4) \times 10^{20}$ cm^{-2} (K km s^{-1})$^{-1}$, while Mead & Kutner (1988) give a value of ∼4 cm^{-2} (K km s^{-1})$^{-1}$. Therefore, we use $X = 8 \times 10^{20}$ cm^{-2} (K km s^{-1})$^{-1}$ keeping in mind that the mass and density may be overestimated by a factor of 2. With these values, the mass and H_2 number density yield $1.2 \times 10^4\ M_\odot$ and 1100 cm^{-3}, respectively.

In Table 2 we summarize the results obtained above. The second column quotes the approximate central position of the structure in equatorial coordinates referred to J2000. The third column lists the radius r after deconvolution with the beam size. The fourth and fifth columns contain the systemic velocity v_{sys} and the FWHM velocity Δv, both in km s^{-1}. The computed mass and H_2 density are given in the last two columns.

3.2. *CTB 37A*

This source (Fig. 3) is actually two SNRs overlapped in projection (Kassim, Baum, & Weiler 1991). One of them, G348.5+0.1 (to the west in Fig. 3), is a partial shell with a

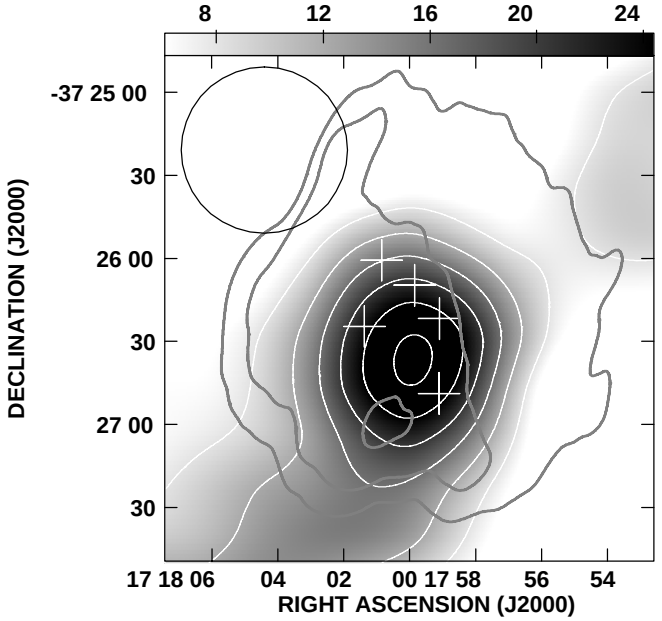

FIG. 2.—CO emission integrated between +14.5 and +18.5 km s^{-1} toward G349.7+0.2, in gray scale and contours. Data were taken with the 12 m telescope of the NRAO. The gray scale is in K km s^{-1} and is shown on top of the image. The white contours represent the CO emission between 8 and 28 K km s^{-1}, in steps of 4 K km s^{-1}. The crosses show the positions of the OH 1720 MHz masers. The beam, 60″ × 60″, is indicated by the open circle in the top left corner. The 3 σ noise level is 6 K km s^{-1}. A few radio continuum contours in gray are included to represent the SNR.

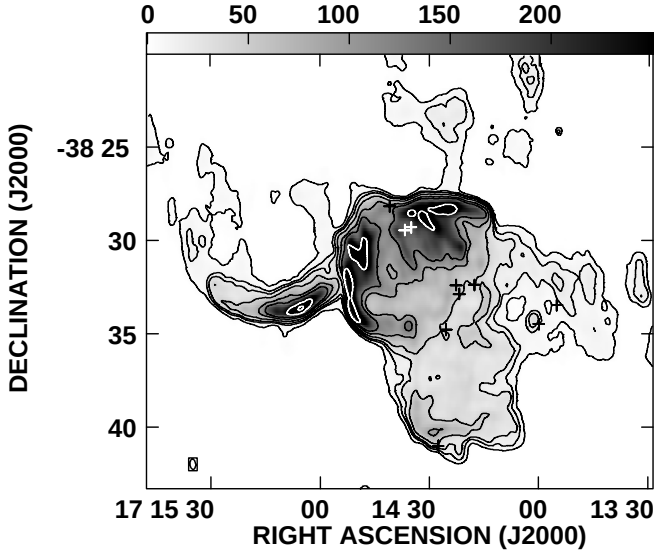

FIG. 3.—Radio continuum image of CTB 37A at 1.4 GHz, from Kassim et al. (1991), obtained with the VLA. Two sources can be identified: G348.7+0.1 to the west, and G348.5−0.0 to the east. The gray scale is indicated in mJy beam^{-1} on top of the image, while the contours are at 1, 3, 5, 10, 20, 30, 65, and 95% of the peak flux. Here again, white contours are used over dark shadows. The peak flux is 0.43 Jy beam^{-1}. Black crosses show the positions of the OH 1720 MHz masers between −63 and −67 km s^{-1}, while white crosses represent the two masers at −25.3 and −22.7 km s^{-1} (Frail et al. 1996). The beam, indicated in the bottom left corner, is 32″.9 × 18″, P.A. = 4°.8.

faint extension out the open end of the shell ("breakout" morphology), while the other one, G348.5−0.0 (to the east in Fig. 3), taken to be a jet of the former by Milne et al. (1979), is a partial shell. By comparing H I spectra of CTB 37A with G349.7+0.2, which is about 1° apart, Caswell et al. (1975) conclude that CTB 37A is beyond the tangential point (at −110 km s^{-1}) but not farther away than a feature seen at −65 km s^{-1}. While most of the OH 1720 MHz masers identified by Frail et al. (1996) appear projected over G348.5+0.1 between −63.5 and −66.3 km s^{-1}, two of them fall at −21.4 and −23.3 km s^{-1} respectively. These two latter masers appear in the region where the two remnants overlap, suggesting that they are associated with G348.5−0.0. Therefore, the OH 1720 MHz masers allow an assignment of the systemic velocities of the two remnants that constitute CTB 37A.

An inspection of the CO emission toward CTB 37A throughout the whole observed velocity range, reveals a very complex distribution. In searching for a positional coincidence among the OH 1720 MHz masers and the CO emission, the best association could be found from −22.7 to −25.3 km s^{-1} (Fig. 4) and from −60.4 to −68.3 km s^{-1} (Fig. 5). In what follows we will describe the identified structures likely to be interacting with the CTB 37A complex.

At about −24 km s^{-1}, a weak CO concentration is observed to the west of G348.5−0.0, with a few brighter clumps embedded. This structure, centered approximately at R.A. = 17^{h}14^{m}39^s, decl. = −38°30′ (J2000), shall be called hereafter "the western cloud". The two OH 1720 MHz masers at −21.4 and −23.3 km s^{-1} lie on the edge of the cloud. A Gaussian fit to the average profile towards the western cloud yields a central velocity of −23.1 km s^{-1} with a FWHM velocity of 5.3 km s^{-1}. At this systemic velocity, the kinematical distance could be 3.1 or 13.5 kpc. If we assume that this cloud is related to the CTB 37A complex, the H I absorption study of Caswell et al. (1975) solves the ambiguity in favor of the larger distance. Regardless of the ambiguity, the Galactocentric distance is 5 kpc.

A value of $X = 2 \times 10^{20}$ cm^{-2} (K km s^{-1})$^{-1}$ will be used in deriving mass and mean H_2 density, based on γ−ray emission studies for the inner Galaxy (Lebrun et al. 1983). Assuming an ellipsoidal geometry with the major and minor axes equal to 340″ and 135″ respectively, the mass is

TABLE 2

OBSERVED AND DERIVED PARAMETERS FOR THE CO STRUCTURE ASSOCIATED WITH G349.7+0.2

CENTRAL COORDINATES						
R.A. (J2000)	Decl. (J2000)	r (arcsec)	v_{sys} (km s^{-1})	Δv (km s^{-1})	M ($M_\odot$)	n_{H_2} (cm^{-3})
17 18 0.....	−37 26 36	24	+16.5	4.0	1.2×10^4	1100

NOTE.—Units of right ascension are hours, minutes, and seconds, and units of declination are degrees, arcminutes, and arcseconds.

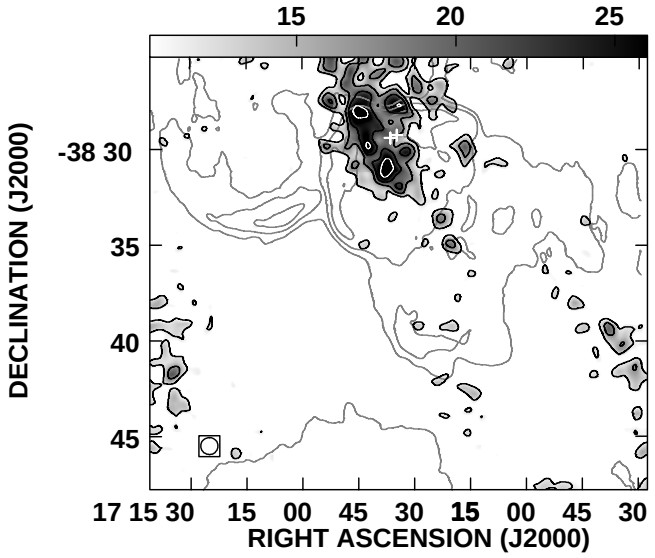

FIG. 4.—CO emission integrated between -25.3 and -22.7 km s^{-1} toward CTB 37A. Data were taken with the 12 m telescope of the NRAO. The gray scale is in K km s^{-1}, and is shown on top of the image. The beam, 53.″6 × 53.″6, is plotted in the bottom left corner. A few representative contours of the continuum emission from CTB 37A are included as gray lines. CO emission contours at 11.5, 17, 22, and 28.5 K km s^{-1} are plotted as black lines, except for the last one which appears in white. The two white plus signs represent the two OH 1720 MHz masers at -21.4 and -23.3 km s^{-1} (Frail et al. 1996). The 3 σ noise level is 9 K km s^{-1}.

estimated to be $\sim 15900\ M_\odot$, and the average H_2 density, 150 cm^{-3}.

Other structures probably associated with the OH 1720 MHz masers are found beyond -60 km s^{-1}. In the integrated image shown in Fig. 5, there is an extended structure covering the north-west half of G348.5+0.1. Several components can be recognized inside this large structure. Because of the proximity with the OH 1720 MHz masers, we will focus on two of them: one centered near R.A. = $17^h14^m20^s.5$, decl. = $-38°33'30''$ (J2000) with three OH 1720 MHz masers on its northern edge, which shall be called "the central cloud"; and another one located to the north, coincident with the continuum shell from R.A. = $17^h14^m50^s.5$, decl. = $-38°27'10''$ (J2000) to R.A. = $17^h14^m17^s.5$, decl. = $-38°30'40''$ (J2000), which shall be called "the northern cloud." Another small, weak cloud, which appears detached from the bulk of the CO emission, will also be studied. This cloud, hereafter called "the southern cloud," is centered approximately at R.A. = $17^h14^m28^s.5$, decl. = $-38°41'50''$ (J2000) and contains an OH 1720 MHz maser on its northern edge.

Since the three clouds are at -65 ± 2 km s^{-1}, we adopt a Galactocentric distance of 3.5 kpc for them, and a kinematical distance of 11.3 kpc, where again we have discarded the closer distance of 5.3 kpc based on the H I absorption results. The central and FWHM velocities of each cloud, as well as the derived masses and densities, are listed in Table 3. In this table, we also include the western cloud at -23.1 km s^{-1}. Units are as in Table 2. In the third column, the listed radii are derived assuming spherical geometries and, where applicable, the correction factor f is included in parenthesis. The northern cloud is assumed to be an ellipsoid enclosed by the outermost white contour in Figure 5. In fitting a Gaussian to the profile towards the central cloud, only the highest peak was taken into account, since the profile looks highly asymmetric and consists of several components. For all the clouds, X was assumed to be equal to 2×10^{20} cm^{-2} (K km s^{-1})$^{-1}$.

3.3. *G16.7+0.1*

G16.7+0.1 (Fig. 6), which belongs to the composite type of SNRs, consists of an irregular shell, brighter to the south, and a central jetlike feature probably powered by an undetected pulsar (Frail & Moffett 1993). Green et al. (1997) detected a single OH 1720 MHz maser near the bright southern edge of the shell, at $+20$ km s^{-1}. Unfortunately, there are no line-absorption studies to constrain the systemic velocity of the remnant and compare it to the velocity of the OH 1720 MHz maser.

Like CTB 37A, G16.7+0.1 appears to be located in a very complex region. The CO emission is extended over a large velocity range. The only feature found at the position of the OH 1720 MHz maser is a small cloud at $\sim +25$ km s^{-1}, centered approximately at R.A. = $18^h20^m56^s.2$, decl. = $-14°21'55''$ (J2000). This feature will be called "the southern cloud." The 5 km s^{-1} gap between the velocities of the OH 1720 MHz maser and the southern cloud, may be related to the anomalous velocity dispersion of the maser, larger than typical values (Green et al. 1997). The southern cloud is seen from $+25.1$ to $+25.9$ km s^{-1}. Figure 7 shows the CO emission integrated over this velocity range.

There are two more structures that seem to be associated with the remnant. One of them is a small concentration inside the shell, centered at about R.A. = $18^h20^m59^s.6$, decl. = $-14°19'22''$ (J2000), located to the east of the central continuum feature. In what follows, we will call this concentration "the central cloud." The other structure is a bright concentration to the northwest, hereafter "the northwestern cloud," centered approximately at R.A. = $18^h20^m46^s.6$, decl. = $-14°18'10''$ (J2000). The close agreement among the contours of the CO and continuum emis-

TABLE 3

OBSERVED AND DERIVED PARAMETERS FOR CO STRUCTURES ASSOCIATED WITH CTB 37A

	CENTRAL COORDINATES						
CLOUD	R.A. (J2000)	Decl. (J2000)	r (arcsec)	v_{sys} (km s^{-1})	Δv (km s^{-1})	M ($M_\odot$)	n_{H_2} (cm^{-3})
Western	17 14 39	−38 30 00	107 (2.5)	−23.1	5.3	1.5×10^4	150
Central	17 14 20.5	−38 33 30	60 (2.1)	−64.0	6.9	7.2×10^3	520
Northern	17 14 30	−38 27 00	150 (3.13)	−65.0	12.0	5.8×10^4	660
Southern	17 14 28.5	−38 41 50	37	−66.6	4.0	1.3×10^3	280

NOTE.—Units of right ascension are hours, minutes, and seconds, and units of declination are degrees, arcminutes, and arcseconds.

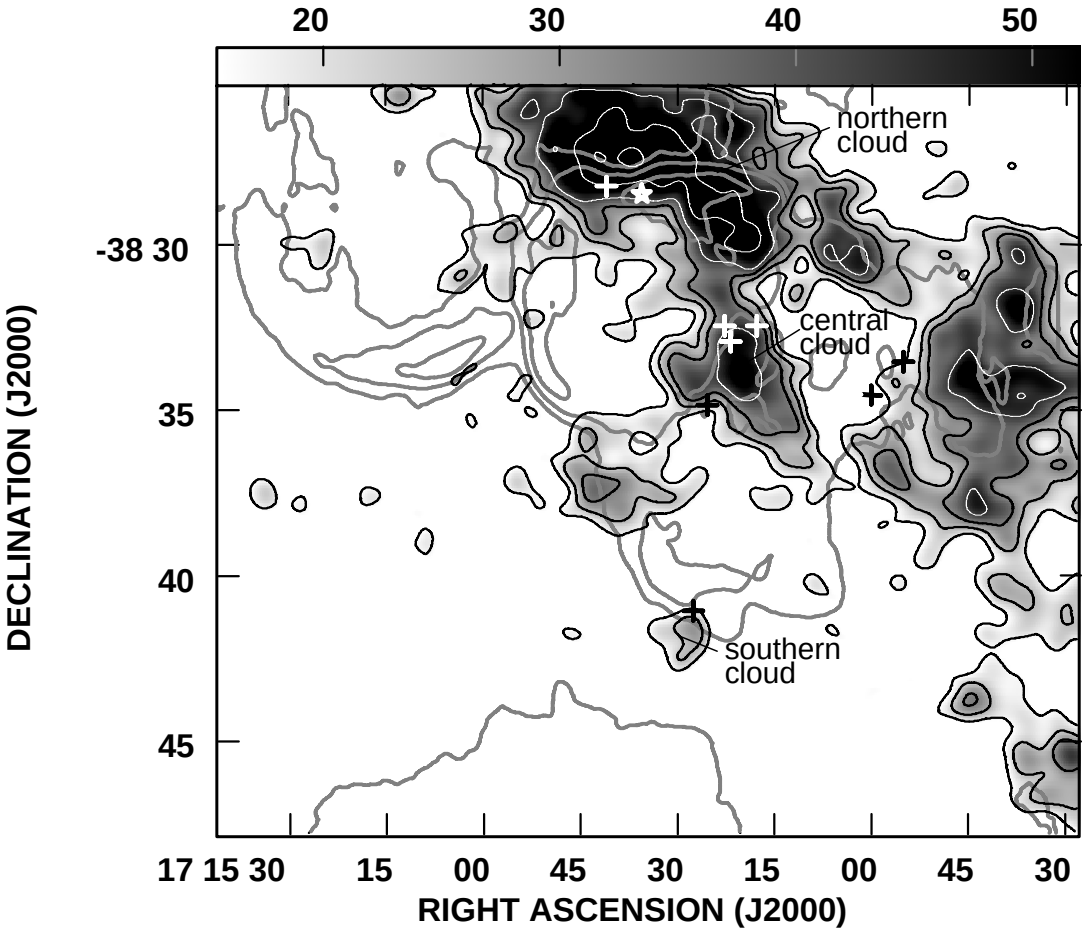

FIG. 5.—CO emission integrated between −68.3 and −60.4 km s^{-1} toward CTB 37A. Data were taken with the 12 m telescope of the NRAO. The gray scale is in K km s^{-1}, and is shown on top of the image. The beam size is 60″ × 60″. A few representative contours of the continuum emission from CTB 37A are included as thick gray lines. CO emission contours at 20, 30, 40, 55, 75, and 95% of the peak emission are plotted in black or white solid lines, according to the darkness of the background. The peak emission is 82.2 K km s^{-1}. The plus signs show the positions of the OH 1720 MHz masers found by Frail et al. (1996) between −63 and −67 km s^{-1}, where white lines have been used over dark background for better contrast. The white star represents the *IRAS* point source 17111−3824 discussed in the text (§ 4.2.2). The arrows indicate the three clouds discussed in the text. The 3 σ noise level is 7 K km s^{-1}.

sion, strongly suggests that the northwestern cloud is causing the flattening of the shock front observed in this direction.

The parameters computed for these three clouds are listed in Table 4. To estimate the distance, we first notice that the peak velocities of the clouds are within 0.2 km s^{-1} of +25.6 km s^{-1}. At +25.6 km s^{-1}, the Galactic rotation model predicts two kinematical distances: 2.6 and 13.7 kpc, and a Galactocentric distance of 3.5 kpc. As stated above, there are no absorption studies to solve the kinematical distance ambiguity. Therefore, we attempted to find which of the two distances is most likely applicable using a Σ-D relationship, in spite of the large intrinsic errors of this method (typical uncertainties can be more than a factor of 2). Based on the surface density given by Helfand et al. (1989), the Σ-D curve estimated by Case & Bhattacharya (1998) produces a distance of 13.7 kpc, in excellent agreement with the farther distance given by the Galactic rotation model. Though this perfect agreement may be a coincidence, the Σ-D distance implies that the lower kinematical distance should be discarded. The ratio X is assumed to be equal to 2×10^{20} cm^{-2} (K km s^{-1})$^{-1}$. The

TABLE 4

OBSERVED AND DERIVED PARAMETERS FOR CO STRUCTURES ASSOCIATED WITH G16.7+0.1

	CENTRAL COORDINATES						
CLOUD	R.A. (J2000)	Decl. (J2000)	r (arcsec)	v_{sys} (km s^{-1})	Δv (km s^{-1})	M ($M_\odot$)	n_{H_2} (cm^{-3})
Southern	18 20 56.2	−14 21 55	32 (1.6)	+25.8	1.5	2.1×10^3	260
Central	18 20 59.6	−14 19 22	28 (1.5)	+25.4	4.4	1.8×10^3	330
Northwestern	18 20 46.6	−14 18 10	37 (2)	+26.6	2.7	3.4×10^3	280

NOTE.—Units of right ascension are hours, minutes, and seconds, and units of declination are degrees, arcminutes, and arcseconds.

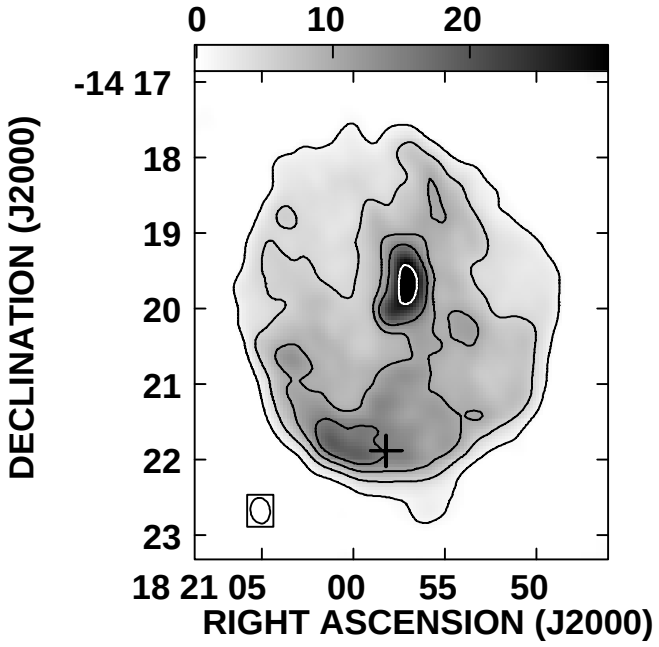

FIG. 6.—Radio continuum image of G16.7+0.1 at 4.86 GHz from Helfand et al. (1989), obtained with the VLA. The gray scale is indicated in mJy beam^{-1} on top of the image, while the contours are at 1, 5, 15, and 30 mJy beam^{-1}. The plus sign indicates the OH 1720 MHz maser detected by Green et al. (1997). The beam, indicated in the bottom left corner, is $21'' \times 16''$, P.A. = 11°.

units are as in Table 2. The third column is as described in Table 3.

4. DISCUSSION

4.1. *Correlation between* CO *Clouds and* OH 1720 MHz *Masers*

To compare quantitatively the agreement between the velocities of the OH 1720 MHz masers and the velocities of the CO peak flux densities, CO profiles toward all individual masers were taken and Gaussian fits to the identified peaks were calculated. The average difference in velocities is $|\Delta V| = 0.6$ km s^{-1}, with a dispersion of 1.7 km s^{-1}. The highest departure, above 5 km s^{-1}, corresponds to G16.7+0.1. Disregarding this latter value, $|\Delta V|$ turns out to be 0.2 ± 1.2 km s^{-1}.

In addition to the velocity agreement, the positional agreement between CO clouds and OH 1720 MHz masers is quite striking in many cases. The best match is found in G349.7+0.2, where all of the masers are aligned around the only CO feature detected towards the remnant. No correlation is found between maser peak flux densities and proximity to the CO emission peak. Brogan et al. (2000) were able to measure magnetic fields of $\sim$300 μG using the Zeeman effect towards the brightest OH masers in this SNR.

Another case in which a very good agreement is found is G16.7+0.1. The OH 1720 MHz maser is not only superimposed on a CO clump (the southern cloud) but also lies at the contact region between the southern cloud and a continuum maximum. However, the velocities are not coincident. According to Green et al. (1997), the maser is at $\sim$ +20 km s^{-1}. The CO images around this velocity show no emission near the position of the OH 1720 MHz maser. In the next paragraph, some suitable explanations for this discrepancy are proposed.

Claussen et al. (1997) found that some of the OH 1720 MHz masers around the SNR W28 do not share the systemic velocity of the remnant, but are blueshifted by $\sim$10 km s^{-1}, as is the molecular gas associated with them. The CO profile towards the southern cloud in G16.7+0.1, shows a weak wing centered at +19.3 km s^{-1}, with a 6.5 km s^{-1} FWHM. This wing, which is in the limit of detectability, would imply that part of the molecular gas of the southern cloud was accelerated to $\sim$6.5 km s^{-1} by the shock wave and, like in the case of W28, the OH 1720 MHz maser indicate the velocity of the accelerated gas. It is also possible that the maser is in fact blended features, as Green et al. (1997) suggested. In such case, it would be important to compare the velocities of split components to the systemic velocity of the southern cloud to analyze the agreement among them.

In CTB 37A, the correlation is poor compared to the other two SNRs. Although the masers are in most cases located inside CO structures, the proximity to emission peaks does not always apply. Moreover, the strength of the masers is unrelated to the local CO emission intensity. There are two masers, located at R.A. = $17^h13^m54^s.87$, decl. = $-38°33'25''.5$ (J2000) and R.A. = $17^h13^m58^s.81$, decl. = $-38°34'26''.2$ (J2000), with velocities -65.1 and -65.2 km s^{-1} respectively, which lie outside the edge of the CO emission region. Brogan et al. (2000) found that, unlike W28 and W44, where magnetic fields are uniform both in magnitude and direction, in CTB 37A the magnetic field strength B_θ changes direction along the line of sight over length scales of only $\sim$3 pc, revealing a complicated magnetic field morphology.

The CO features found with the present data to be associated with the OH 1720 MHz masers, have densities not higher than $\sim 10^3$ cm^{-3}, which is at least 2 orders of magnitude lower than theoretical predictions. The ^{12}CO $J = 1$–0 line is highly saturated toward the dense center of molecular clouds, and thus does not vary linearly with the column density (Oka et al. 1998). However, low-density cloud envelopes, which are less opaque, are sensitively traced by this line. Since most of the material in a cloud resides in the envelopes, this line is adequate to estimate a reliable mass for the cloud. To detect high-density clumps or cores inside clouds, with densities in the range 10^4–10^6 cm^{-3}, other species like CS, C^{18}O, or H_2CO (Mangum & Wootten 1993; Bronfman, Nyman, & May 1996) or higher CO transitions (e.g., Frail & Mitchell 1998) need to be observed. Frail & Mitchell (1998) estimated the densities of postshock gas associated with OH 1720 MHz masers to be $n_{H_2} \sim 10^4$–10^6 cm^{-3}, and infer preshock densities of the order 10^2–10^3 cm^{-3}. In summary, our data reveal the ISM structures with which SNRs are interacting, but do not probe the shocked molecular gas in which the OH 1720 MHz maser emission is produced, which should be observed in other lines.

4.2. *Interaction between SNRs and Molecular Clouds*

Large molecular complexes are proposed to be the birthplace of the young, massive progenitor stars of Type II supernovae. Half of the Galactic SNRs are supposed to be of this type, and this would be the reason why Huang & Thaddeus (1986) found a very good correlation between large molecular cloud complexes and half of the SNRs sur-

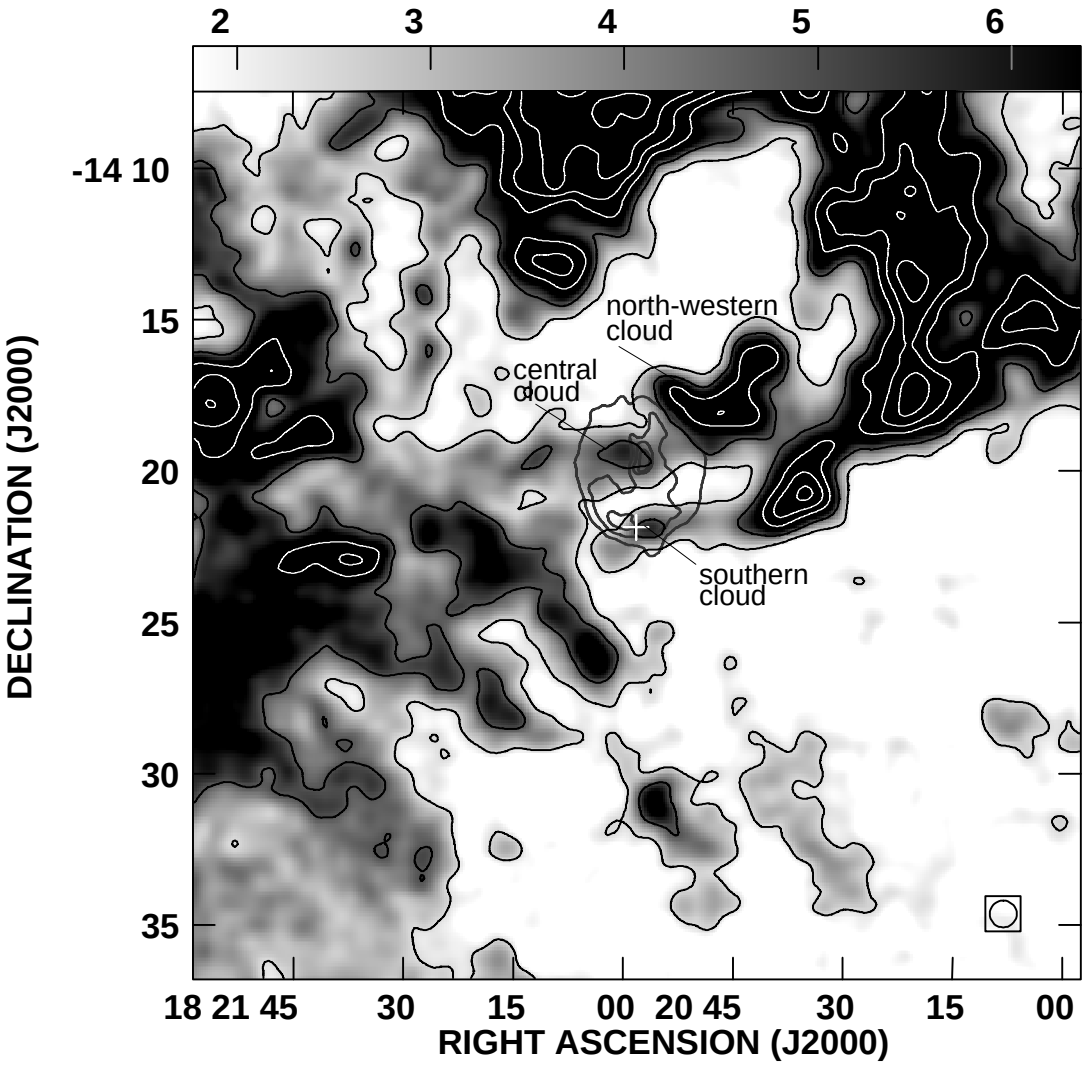

FIG. 7.—CO emission integrated between −25.1 and −25.9 km s^{-1} toward G16.7+0.1. Data were taken with the 12 m telescope of the NRAO. The gray scale is in K km s^{-1} and is shown on top of the image. The beam size, 53″.6 × 53″.6, is plotted in the bottom right corner. A few representative contours of the continuum emission from G16.7+0.1 are included as dark-grey lines. CO emission contours at 3.8, 7.6, 12.7, 16.5, 20.3, and 24 K km s^{-1} are plotted in black and white solid lines, according to the darkness of the background. The plus sign in white shows the position of the OH 1720 MHz maser found by Green et al. (1997). The arrows indicate the three clouds discussed in the text. The 3 σ noise level is 1.5 K km s^{-1}.

veyed in CO. It is likely that the observed molecular complexes be part of the natal-clouds of the presupernova stars. However, although it is statistically improbable that such a good correlation arises from chance superpositions, there is very little direct evidence that SNRs are actually in physical contact with the molecular clouds observed.

Shocked-excited 1720 MHz OH masers toward SNRs constitute a powerful tool to ensure on safe grounds that the molecular structures at the same velocity of the masers are physically related to the remnants. The use of OH 1720 MHz masers as signposts of SNR–molecular cloud interactions allowed us to detect the molecular gas into which SN shock fronts are being driven. In what follows, we analyze the interaction of each SNR with its surrounding molecular gas.

4.2.1. *G349.7+0.2*

In this case, the evidence for SNR–molecular cloud interaction is compelling, based on the positional and velocity coincidence between the CO feature and the OH 1720 MHz masers. This conclusion supports the statement of Clark & Caswell (1976) that the expansion has been influenced by a dense environment in early stages. To obtain an additional proof of interaction, we have searched for *IRAS* point sources that fulfill the following conditions: (1) $S_{100} \geq 20$ Jy, (2) $1.2 \leq S_{100}/S_{60} \leq 6.0$, and (3) $S_{60}/S_{25} \geq 1$, where S_λ denotes the (uncorrected) IR-flux density in the wavelength λ μm. These selection criteria are indicative of protostars (Junkes, Fürst, & Reich 1992) or dust heated in SNR shocks (Arendt 1989). We have found that the point source IRAS 17146−3723, which agrees with these conditions, is positionally coincident with the CO cloud. It is unlikely that this *IRAS* source is a protostar triggered by the shock wave of G349.7+0.2 because of the timescales involved. Formation of protostars from condensed molecular matter needs a period of the order of 10^6 yr, enough for the matter to cool, which is too long compared to the age of a SNR. We therefore suggest that IRAS 17146−3723 is produced by shock-

heated dust and, together with the OH 1720 MHz maser emission, confirms the interaction between the SNR and the molecular cloud detected here. A thorough analysis of the more extended region surveyed here is given in Reynoso & Mangum (2001)

4.2.2. *CTB 37A*

Our observations show two distinct clouds towards CTB 37A, both coincident spatially and in velocity with the two groups of OH 1720 MHz masers. Thus, the present CO data provide additional support to the theory of the two overlapped SNRs. However, the complexity of the CO distribution in this direction makes it difficult to identify molecular clouds interacting with the SNR shock fronts. One of the remnants, G348.5+0.1, has a characteristic "breakout" morphology, which would imply a strong density gradient. Nevertheless, there is no correspondence between the CO distribution and such radio morphology. This is in contrast with the case of 3C 391, where the ^{12}CO distribution shows a molecular cloud exactly parallel to the bright radio emission ridge (Wilner et al. 1998). As in the case of G349.7+0.2, an additional evidence for interaction is given by the *IRAS* point source 17111−3824, which has an IR spectrum typical of shocked heated dust according to the criteria of Junkes et al. (1992), and lies close to the OH maser at the northern cloud. This *IRAS* source is shown as a white star in Fig. 5.

Apart from the presence of the OH 1720 MHz masers and IRAS 17111−3824, there are no further indications of shocked molecular gas such as line broadenings or wings. However, at ~ -88 km s^{-1} there appears a bright, elongated CO structure positionally following the masers closest to the central cloud. In Figure 8, two profiles are shown, the upper towards the three masers at the central cloud (white crosses in Fig. 5), and the lower towards an arbitrary direction displaced from the remnant, at the northwest of the field. In the upper profile, three peaks are clearly distinguished: one at ~ -65 km s^{-1}, which corresponds to the gas in which the OH 1720 MHz masers originate, and the others at approximately -88 and -107 km s^{-1}. The peak at ~ -107 km s^{-1} is also seen in the profile outside the SNR, and is commonly regarded as an expanding arm about 3 kpc from the Galactic center (Caswell et al. 1975). The other peak, instead, does not appear in the lower profile, so it is likely to be related with the central cloud. At -88 km s^{-1}, the only CO emission observed extends over the area enclosed by the radio continuum emission. Therefore, we propose that the CO emission at this velocity corresponds to a fraction of molecular gas accelerated by the shock front at a velocity of about 25 km s^{-1}. This accelerated component of the gas would be additional proof for an SNR–molecular cloud interaction.

Chevalier (1999) proposes that in the initial interaction, the (radiative) SNR shell drives a slab into the cloud. We suggest that in this case, the slab can be seen as the -88 km s^{-1} component. The postshock pressure is $\rho_{cl} v_{cl}^2 \simeq 8 \times 10^{-9}$ dyn cm^{-2}, where the subindex *cl* indicates that the parameters are estimated at the cloud. Assuming constant density for the radiative shell, and allowing for magnetic fields, Chevalier's model states that the ratio between the ram pressure in the slab and that at the front of the radiative shell, $\rho_{cl} v_{cl}^2 / \rho_0 v_{rs}^2$, is limited to the range $\sim$10–100. In this equation, ρ_0 is the intercloud density and v_{rs} is the velocity of the radiative shell before entering the cloud.

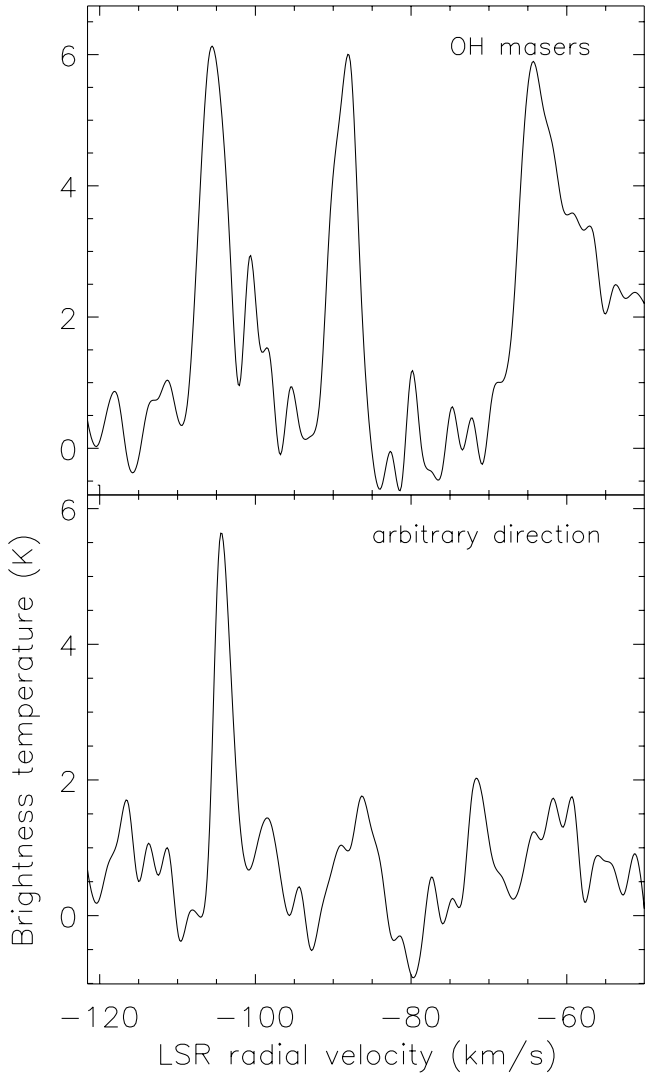

FIG. 8.—CO emission profiles toward the OH masers lying on the central cloud in CTB 37A (*upper profile*) and towards an arbitrary direction, to the northwest of the observed field and displaced from the continuum emission (*lower profile*). Brightness temperatures are in Kelvins, while velocities are in km s^{-1}.

Thus, assuming $n_0 = 15$ cm^{-3} as a typical value for the intercloud density (e.g., Chevalier 1999), the shock velocity at the cloud is $\sim$15–30 km s^{-1}. At velocities lower than $\sim$50 km s^{-1}, shocks are of C-type (Neufeld & Dalgarno 1989); thus this estimate is consistent with the theoretical prediction by Lockett et al. (1999) that the conditions under which 1720 MHz OH maser emission is produced can exist only if shocks are of C-type. An upper limit of $v_{rs} = 60$ km s^{-1} can be reached if an intercloud density as low as $n_0 = 1$ cm^{-3} (e.g., McKee & Cowie 1975; Dubner et al. 1999) is assumed.

4.2.3. *G16.7+0.1*

Like G349.7+0.2, this is another case in which the evidence for SNR–molecular cloud interaction is clear. What is remarkable about this case is that one single maser was found to be associated with a region with several structures of molecular gas and more than one site of possible interaction between this gas and the SNR shock front. The same

occurs with IC 443 which, in spite of being one of the remnants more clearly interacting with dense molecular gas, has only one maser coincident with a site where the shock is transverse (Claussen et al. 1997).

Based on high-resolution observations, Frail & Moffett (1993) describe the central jetlike radio structure as consisting of a center of symmetry at R.A. = $18^h20^m57^s.48$, decl. = $-14°19'57''.6$ (J2000) from which emission extended in two directions opens up into more extended lobes. In Figure 7 it can readily be seen that the northern lobe seems to be inclined towards the central cloud, tending to enclose the inner CO emission peak (see also Fig. 6). Also, the southern lobe appears to the east of the southern cloud, with the OH 1720 MHz maser lying at the contact region between them. Both lobes show enhancements in the radio continuum emission at the locations of the molecular clouds, which is an indication of interaction.

In virtue of the morphological agreement, the northwestern cloud appears to be an excellent candidate for interaction with this SNR, although no line broadenings are detected. The interaction between G16.7+0.1 and the northern cloud places this remnant in the same class as IC 443 and 3C 391 in the sense that, although the morphologically most convincing site of SNR–molecular gas interaction is suggested by a flat radio continuum rim exactly parallel to the boundary of a molecular cloud, there appears only one maser (actually two in the case of 3C 391), and not at that site but near the opposite side of the remnant. Moreover, the morphology involved in such cases makes it difficult not to conceive a strongly transverse shock. Thus, it appears that not all transversely shocked dense gas regions lead to the conditions that give rise to OH 1720 MHz maser emission. Possible explanations for the lack of OH 1720 MHz masers in these cases could be related, for instance, to dissociation of OH by high-velocity shocks. The trend observed in these three remnants is undoubtedly a topic that deserves further investigation, and should certainly be taken into account in future theoretical works.

5. CONCLUSIONS

The surroundings of the SNRs G349.7+0.2, CTB 37A and G16.7+0.1 have been investigated in the CO $J = 1–0$ transition. These remnants have been selected since all of them have associated OH 1720 MHz maser emission. Our observations allowed us to determine the density distribution of the ISM into which these remnants are expanding, revealing a rich environment in all three cases. In spite of the confusion produced by the ubiquity of the CO $J = 1–0$ emission, we have been able to identify molecular clouds interacting with SNRs based mainly on the positional and kinematical coincidence with shock-excited OH 1720 MHz masers, but also on morphological arguments as well as radio continuum enhancements, IR emission by shock-heated dust, and peculiar spectral components. Unfortunately, we have not detected spectral line broadenings, which are unmistakable signatures of interaction. However, there are other cases of SNRs interacting with molecular clouds, in which no line broadenings have been observed in the CO $J = 1–0$ transition (Wilner et al. 1998; Dubner et al. 1999). Reasons for this nondetection vary from rapid dissociation of the molecules, masking of weak CO $J = 1–0$ features by background cloud emission, and beam dilution of highly localized blast-wave interactions (Wilner et al. 1998).

The main results of this paper are summarized below.

1. All but two of the OH 1720 MHz masers are associated with CO emission peaks that possess an excellent velocity correlation with the former. The difference between both velocities is in average (0.6 ± 1.7) km s^{-1} in the worst case.
2. The masers are positionally close to, but not coincident with, CO peaks. The same trend has been observed by Frail & Mitchell (1998).
3. The CO emission associated with the OH 1720 MHz masers allows constraint of the systemic velocities of the SNRs.
4. The H_2 densities inferred ($\leq 10^3$ cm^{-3}) are representative of the preshock gas but do not trace high-density clumps or shocked, compressed material.
5. Several cases of SNR–molecular cloud interaction have been detected based on wings, shifted spectral components, morphological coincidences, and IR emission from shock-heated dust.
6. In G16.7+0.1, the OH 1720 MHz maser seems to originate in molecular gas accelerated to 6.5 km s^{-1}, not in the gas located at the systemic velocity of the SNR.
7. The interstellar gas does not account for the breakout morphology of G348.5+0.1, one of the SNRs of the CTB 37A complex.
8. In CTB 37A, the shock is computed to be of C-type, in agreement with theoretical predictions (Lockett et al. 1999).
9. G16.7+0.1 is found to belong to a group of SNRs (together with 3C 391 and IC 443) with the following common characteristic: part of the rim is obviously flattened by a dense molecular cloud. The morphology strongly suggests that the expansion is perpendicular to the line of sight at this location. However, no OH maser emission at 1720 MHz is detected. The only OH 1720 MHz masers observed in such remnants (only one or two) are far from the flattened part of the rim. This behavior seems to contradict the suggestion that OH 1720 MHz masers appear where shocks are transverse.

We are grateful to the NRAO for allocating time in the 12 Meter Telescope for this project. We also thank D. Helfand, N. Kassim, and C. Salter for providing us their continuum images of the SNRs. E. M. R. acknowledges travel grant 1526/98 from CONICET (Argentina) for visiting the 12 m telecope, as well as NRAO support and staff assistance during her visit. This research was partially funded through a Cooperative Science Program between CONICET and NSF and through CONICET grant 4203/96.

REFERENCES

Allen, C. W. 1973, Astrophysical Quantities (3d ed.; London: Athlone)
Arendt, R. 1989, ApJS, 70, 181
Brogan, C. L., Frail, D. A., Goss, W. M., & Troland, T. H. 2000, ApJ, 537, 875
Bronfman, L., Nyman, L.-Å., & May, J. 1996, A&AS, 115, 81
Burton, M. G., Brand, P. W. J. L., Geballe, T. R., & Webster, A. S. 1988, MNRAS, 231, 617
Case, G. L., & Bhattacharya, D. 1998, ApJ, 504, 761
Caswell, J. L., Murray, J. D., Roger, R. S., Cole, D. J., & Cooke, D. J. 1975, A&A, 45, 239
Chevalier, R. A. 1999, ApJ, 511, 798
Clark, D. H., & Caswell, J. L. 1976, MNRAS, 174, 267
Claussen, M. J., Frail, D. A., Goss, W. M., & Gaume, R. A. 1997, ApJ, 489, 143

DeNoyer, L. K. 1979a, ApJ, 228, L41
———. 1979b, ApJ, 232, L165
———. 1983, ApJ, 264, 141
Digel, S. W., Bally, J., & Thaddeus, P. 1990, ApJ, 357, L29
Digel, S. W., Hunter, S. D., Mukherjee, R., De Geus, E. J., Grenier, I. A., Heithausen, A., Kanbach, G., & Thaddeus, P. 1997, in IAU Symp. 170, CO: Twenty-Five Years of Millimeter-Wave Spectroscopy, ed. W. B. Latter et al. (Dordrecht: Kluwer), 22
Dubner, G. M., Giacani, E. B., Reynoso, E. M., Goss, W. M., Roth, M., & Green, A. J. 1999, AJ, 118, 930
Elitzur, M. 1976, ApJ, 203, 124
Fich, M., Blitz, L., & Stark, A. A. 1989, ApJ, 324, 272
Frail, D. A., Goss, W. M., Reynoso, E. M., Giacani, E. B., Green, A. J., & Otrupcek, R. 1996, AJ, 111, 1651
Frail, D. A., Goss, W. M., & Slysh, V. I. 1994, ApJ, 424, L111
Frail, D. A., & Mitchell, G. F. 1998, ApJ, 508, 690
Frail, D. A., & Moffett, D. A. 1993, ApJ, 408, 637
Goss, W. M. 1968, ApJS, 15, 131
Goss, W. M., & Robinson, B. J. 1968, Astrophys. Lett., 2, 81
Green, A. J., Frail, D. A., Goss, W. M., & Otrupcek, R. 1997, AJ, 114, 2058
Hardebeck, E. G. 1971, ApJ, 170, 281
Helfand, D. J., Velusamy, T., Becker, R. H., & Lockman, F. J. 1989, ApJ, 341, 151
Huang, Y.-L., & Thaddeus, P. 1986, ApJ, 309, 804
Junkes, N., Fürst, E., & Reich, W. 1992, A&A, 261, 289
Kassim, N. E., Baum, S.A., & Weiler, K. W. 1991, ApJ, 374, 212
Koralesky, B., Frail, D. A., Goss, W. M., Claussen, M. J., & Green, A. J. 1998, AJ, 116, 1323
Landecker, T. L., Pineault, S., Routledge, D., & Vaneldik, J. F. 1989, MNRAS, 237, 277
Lebrun, F., et al. 1983, ApJ, 274, 231
Lockett, P., Gauthier, E., & Elitzur, M. 1999, ApJ, 511, 235
Mangum, J. G., & Wootten, A. 1993, ApJS, 89, 123
McKee, C. F., & Cowie, L. L. 1975, ApJ, 195, 715
Mead, K. N., & Kutner, M. L. 1988, ApJ, 330, 399
Milne, D. K., Goss, W. M., Haynes, R. F., Wellington, K. J., & Caswell, J. L. 1979, MNRAS, 188, 437
Neufeld, D. A., & Dalgarno, A. 1989, ApJ, 340, 869
Oka, T., Hasegawa, T., Hayashi, M., Handa, T., & Sakamoto, S. 1998, ApJ, 493, 730
Reach, W. T., & Rho, J. 1998, ApJ, 507, L93
———. 1999, ApJ, 511, 836
Reynoso, E. M., Dubner, G. M., Goss, W. M., & Arnal, E. M. 1995, AJ, 110, 318
Reynoso, E. M., & Mangum, J. G. 2001, AJ, in press
Seta, M., et al. 1998, ApJ, 505, 286
Turner, B. E. 1969, ApJ, 157, 103
White, G. J., Rainey, R., Hayashi, S. S., & Kaifu, N. 1987, A&A, 173, 337
Wilner, D. J., Reynlolds, S. P., & Moffett, D. A. 1998, AJ, 115, 247
Wootten, A. 1977, ApJ, 216, 440
———. 1981, ApJ, 245, 105